Geophysical Journal International

Geophys. J. Int. (2016) **207,** 562–570
Advance Access publication 2016 August 8
GJI Seismology

doi: 10.1093/gji/ggw298

Inversion for seismic moment tensors combining translational and rotational ground motions

S. Donner, M. Bernauer and H. Igel

Department of Earth and Environmental Sciences, LMU Munich, Munich, Germany. E-mail: donner@geophysik.uni-muenchen.de

Accepted 2016 August 3. Received 2016 July 20; in original form 2015 November 20

SUMMARY

We assess the potential of additional rotational ground motions to increase the resolution of the full seismic moment tensor and its centroid depth during waveform inversion. For this purpose, we set up a test case of a shallow, medium-sized strike-slip source. In two scenarios, one based on theoretical station distribution and the other based on real station distribution, we compare the results based on inversion of translational ground motion data only and based on both, translational and rotational ground motion data. The inversion is done with a Bayesian approach to overcome the drawbacks of deterministic approaches and provide a comprehensive quantification of uncertainties. Our results indicate that the resolution of the moment tensor can be increased drastically by incorporating rotational ground motion data. Especially, the usually problematic components M_{xz} and M_{yz} as well as all components containing spatial derivatives with depth benefit most. Also, the resolution of the centroid depth is much better.

Key words: Inverse theory; Earthquake ground motions; Earthquake source observations; Rotational seismology.

1 INTRODUCTION

1.1 Difficulties in seismic moment tensor retrieval

Seismic moment tensors for point sources are an important tool for several applications in seismology. The probably two most important applications is their analysis for seismotectonic studies and their usage as input data for tomographic studies. The successful inversion of waveforms for seismic point-source moment tensors depends on several factors. Especially, in the regional and local distance range, for example, the lack of an appropriate velocity model, a sparse network of stations, or a low signal-to-noise ratio combined with more complex waveforms than in teleseismic distances hamper the comprehensive retrieval of seismic moment tensors.

In the regional distance range waveform inversion is usually done on the surface waves because of their dominant amplitudes in the frequency range below 1 Hz. Higher frequencies very often are not suitable because a quite detailed velocity model would be needed which is often not available. Unfortunately, the equations for the radiation pattern of Love and Rayleigh waves contain coefficients including spatial derivatives of the eigenfunctions with respect to depth. They are proportional to the shear traction on a horizontal plane which is vanishing at the free surface. Thus, for shallow earthquakes (depth $\ll$ wavelength) the moment tensor components M_{xz} and M_{yz}, connected to the coefficients in question, are not very well resolved by waveform inversion. As a consequence, a shallow mechanism can only be uniquely determined from long-period surface waves if one of the nodal planes is subhorizontal (Dufumier & Cara 1995; Bukchin 2006; Bukchin *et al.* 2010). In addition, performing full waveform inversion for moment tensors in a frequency range suitable for surface waves in northern Iran, we also observed instabilities in the resolution of the components M_{xx} and M_{yy}, causing a bias of strike-slip mechanisms tending to thrust mechanisms (e.g. Donner *et al.* 2013).

1.2 Rotational ground motions

To describe the complete wavefield excited by an infinitesimal deformation, three components of translation, three components of rotation, and six components of strain are required (Aki & Richards 2002). So far, seismological studies are mainly based on measurements of translation, sometimes complemented by measurements of strain. For a long time rotational motions have been ignored because of the lack of suitable measurement devices and the misinterpretation of the rotational part of the strain tensor. However, devices based on fibre-optic techniques to measure three-component rotational ground motions are within reach (Schreiber *et al.* 2009; Bernauer *et al.* 2012).

Rotational ground motions are excited by the earthquake source process as well as by interaction of the wavefield with heterogeneities of the Earth. Rotation $\vec{\omega}$ is defined through a linear

combination of space derivatives of the translation vector $\vec{u} = (u_x, u_y, u_z)$:

$$\begin{pmatrix} \omega_x \\ \omega_y \\ \omega_z \end{pmatrix} = \frac{1}{2} \begin{pmatrix} \partial_x \\ \partial_y \\ \partial_z \end{pmatrix} \times \begin{pmatrix} u_x \\ u_y \\ u_z \end{pmatrix} = \frac{1}{2} \begin{pmatrix} \partial_y u_z - \partial_z u_y \\ \partial_z u_x - \partial_x u_z \\ \partial_x u_y - \partial_y u_x \end{pmatrix}, \quad (1)$$

where $\times$ denotes a vector product. The horizontal components of the rotation vector, also known as tilt, carry information on the seismic wavefield at depth. Relying only on translational measurements from conventional station networks this information is not available.

1.3 Motivation and outline

Anticipating the availability of six-component (6-C) seismic arrays, the goal of this study is to investigate the benefits of rotational ground motion for inversion for seismic point-source moment tensors. Especially, the effects of reducing the number of stations by half (but keeping the amount of data constant) will be the focus. If half the number of 6-C stations will provide us with at least comparable if not better results compared to 3-C stations, this would be a success and of great importance considering, for example, the maintenance efforts for a seismic network.

Following the approach of Bernauer *et al.* (2014), we apply a Bayesian, that is, probabilistic, inversion approach. Thus, we can combine different data types in a natural way and are able to quantify the information gain that results from the inversion with and without considering rotational ground motions.

Iran is one of the most threatened countries concerning seismic hazard. The northern part of the country, the Alborz mountains along the coast of the South Caspian Basin, is the most densely populated region including the capital Tehran. Here, about 30 per cent of Iranians population (about 24 millions) is living on about 5 per cent of the country's area (Statistical Centre of Iran 2012; Maps of the World 2013). Also much of the industrial infrastructure is concentrated here. From historical seismicity it is known that the largest seismic events in Iran with inferred magnitudes $M > 7$ have occurred here (Berberian 2014). However, the rate of seismicity is low; strain is released by strong but rare earthquakes (Zamani & Agh-Atabai 2009). Due to this and other reasons a comprehensive retrieval of seismic moment tensors in this region is aggravated (e.g. Donner *et al.* 2014). Therefore, we consider it to be the ideal test case region for our study and set up our synthetic scenario here.

In the following, we first introduce the parametrization of the synthetic earthquake scenario placed in northern Iran. We have chosen a very shallow event on a steep fault plane to involve all the difficulties known from conventional inversion. Second, we very briefly describe the Bayesian inversion approach. The next section is then dedicated to several test inversions for the six moment tensor components and depth. We tested a scenario based on theoretical station locations to analyse the general power of using rotational ground motions for inversion for moment tensors. Thereafter, we performed the inversion based on the real station distribution of the Iranian broadband network. In both cases, we performed the inversion with only using theoretical data from 3-C stations compared to using theoretical data from half the number of 6-C stations. We conclude with a discussion on the resolvability of moment tensor components and centroid depths for both scenarios. Also, the stability of the decomposition of the resulting moment tensors is discussed.

Table 1. Parameters of the synthetic earthquake source.

Lat (°)	35.2	M_{xx}	− 0.75
Lon (°)	53.2	M_{xy}	− 0.16
Depth (km)	6.0	M_{xz}	0.41
M_w	4.0	M_{yy}	1.17
Strike/dip/rake (°)	228/65/-10	M_{yz}	0.26
(Auxiliary)	322/81/-155	M_{zz}	0.02
DC/ISO/CLVD (per cent)	80/15/5		

Table 2. Description of the layered Earth model used for wavefield computation.

Layer (km)	v_P (km s^{-1})	v_S (km s^{-1})	Density (g cm^{-3})	Q_P	Q_S
0	4.60	2.69	2.41	580	300
3	5.48	3.16	2.58	580	300
8	5.94	3.29	2.69	580	300
14	6.33	3.49	2.80	580	300
18	6.53	3.57	2.86	580	300
48	8.07	4.16	3.33	973	484
80	8.10	4.18	3.48	973	484

Properties are constant within individual layers. Q values are taken from Pasyanos *et al.* (2009a,b).

2 THE SYNTHETIC EARTHQUAKE SCENARIO

We set up a scenario with a synthetic earthquake having an almost pure vertical strike-slip mechanism at the southeastern part of the Alborz mountains, northern Iran. At this region similar earthquake mechanisms with magnitudes as large as $M \sim 6$ have been observed in recent times. Our synthetic example is placed in a depth of 6 km with a magnitude of M_w 4.0, and a double-couple (DC) percentage of 80 per cent. The DC part of the moment tensor was determined from fictionally chosen strike ($\phi = 228°$), dip ($\delta = 65°$), and rake angles ($\lambda = -10°$) according to eq. (18) of Jost & Herrmann (1989). The full theoretical moment tensor is then obtained by weighting the DC moment tensor with the factor 0.8 and adding 0.15 times an isotropic (ISO) and 0.05 times a compensated linear vector dipole (CLVD) moment tensor. Further details of the source can be found in Table 1.

The theoretically observed waveforms are computed based on the 1-D structural model for the Alborz mountains (Table 2; Donner *et al.* 2013). To be flexible for potentially more complex studies in the future, we applied a spectral-element solver (Fichtner *et al.* 2009). The wavefield is computed up to a frequency of 0.1 Hz with a minimum wavelength of 27 km. Thus, we are able to simulate the inversion of surface waves as it is usually done in the regional distance range. The forward problem for the seismic point-source moment tensor according to Aki & Richards (2002) is given as:

$$u_n(\mathbf{x}, t) = M_{kj} \cdot G_{nk,j}(\mathbf{x}, t - \tau) \quad (2)$$

with u_n being the ground motion at observation point $\mathbf{x}$ and time t, M_{kj} being the components of the seismic moment tensor and $G_{nk,j}$ being the spatial derivatives of the Green's function components. τ is the origin time of the source. Einstein summation convention was applied to facilitate readability of the equation. Because we used a delta pulse as (fixed) source time function the underlying convolution of this equation can be simplified to a multiplication (Jost & Herrmann 1989). Depending on what kind of ground motion is used as u_n (displacement, velocity, rotation) the Green's functions have to be calculated correspondingly.

To be more realistic, we added Gaussian noise to each synthetic seismogram. The noise on the translational and rotational

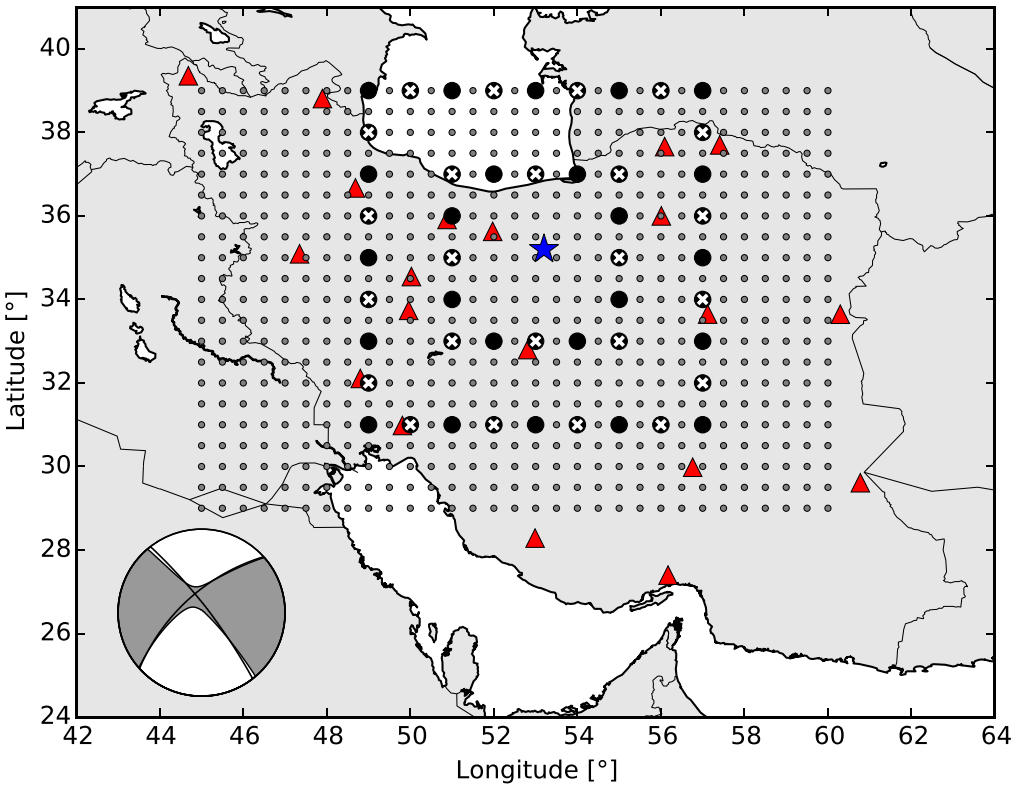

Figure 1. Overview map of Iran. Grey dots show a regular net of theoretical station locations used for randomized generalization while black and white-crossed dots mark selected stations for inversion scenario I (see the text for further explanation). Red triangles mark the real station distribution of INSN network. The location of the theoretical event is given by a blue star. The theoretical mechanism is shown in the lower left corner with grey and black being the full moment tensor and the DC part only, respectively.

components is not correlated due to a wave equation solver which directly calculates translational and rotational seismograms. For our study only the relative noise levels in the two kinds of data are relevant. We set a unique noise level of 10 per cent of the maximum amplitude observed in the data, evaluating translational and rotational ground motions separately because of their huge amplitude differences. Thus, any potential gain or loss of information during inversion does not result from different noise levels. The choice of 10 per cent is arbitrary. However, Bernauer *et al.* (2014) stated that the noise levels in both data sets should be similar.

For the first test based on a theoretical distribution of stations, we distributed two rings of stations around the source in distances of about 220 km and 448 km simulating an optimal azimuthal coverage (Fig. 1). Here, we compared the results of inverting theoretical waveform data from 48 3-C (black dots) versus 24 6-C stations (black dots with additional white crosses). To generalize the findings, we then performed 1000 inversions using data of the same amount of stations randomly selected out of a regular grid marked by grey dots in Fig. 1.

In a second test, we used the real station distribution of the Iranian National Seismic Network (INSN) operated by the International Institute of Earthquake Engineering and Seismology (IIEES) in Tehran (Fig. 1 and Table 3).

Table 3. Stations of the Iranian permanent broad-band network INSN.

#	Station	Lat (°)	Lon (°)	#	Station	Lat (°)	Lon (°)
1	ASAO	34.55	50.03	11	NASN	32.80	52.81
2	BNDS	27.40	56.17	12	RMKL	30.98	49.81
3	BJRD	37.70	57.49	13	SHGR	32.11	48.80
4	DAMV	35.63	51.97	14	SHRD	36.00	56.01
5	GHIR	28.29	52.99	15	SHRT	33.65	60.30
6	GRMI	38.81	47.89	16	SNGE	35.09	47.35
7	KHMZ	33.74	49.96	17	TABS	33.65	57.12
8	KRBR	29.98	56.76	18	THKV	35.92	50.88
9	MAKU	39.35	44.68	19	ZHSF	29.61	60.78
10	MRVT	37.66	56.09	20	ZNJK	36.67	48.69

3 PROBABILISTIC WAVEFORM INVERSION FOR SEISMIC MOMENT TENSORS

Deterministic source inversion is based on finding the solution which best explains the data, usually by an iterative approach. This procedure often includes a selection of the solution according to the lowest inversion residual, which not necessarily is the most reliable one (Bean *et al.* 2008; Donner *et al.* 2014). Further solutions explaining the data equally well are neglected. An estimate of the solution error is rarely given.

Although computationally more expensive, a probabilistic (or Bayesian) inversion approach overcomes the mentioned drawbacks using a global model search. Thus, a Bayesian approach provides unbiased measures of resolution and possible trade-offs.

In our study, we use the same Bayesian inversion approach described in Bernauer *et al.* (2014) based on equations from Tarantola (2005):

$$\sigma(\mathbf{m}) = k\rho(\mathbf{m})L(\mathbf{m}), \tag{3}$$

where $\sigma(\mathbf{m})$ and $\rho(\mathbf{m})$ are the *posterior* and *prior probability density functions* (pdf) on the model parameters, respectively, k is a normalization constant, and $L(\mathbf{m})$ is the likelihood function

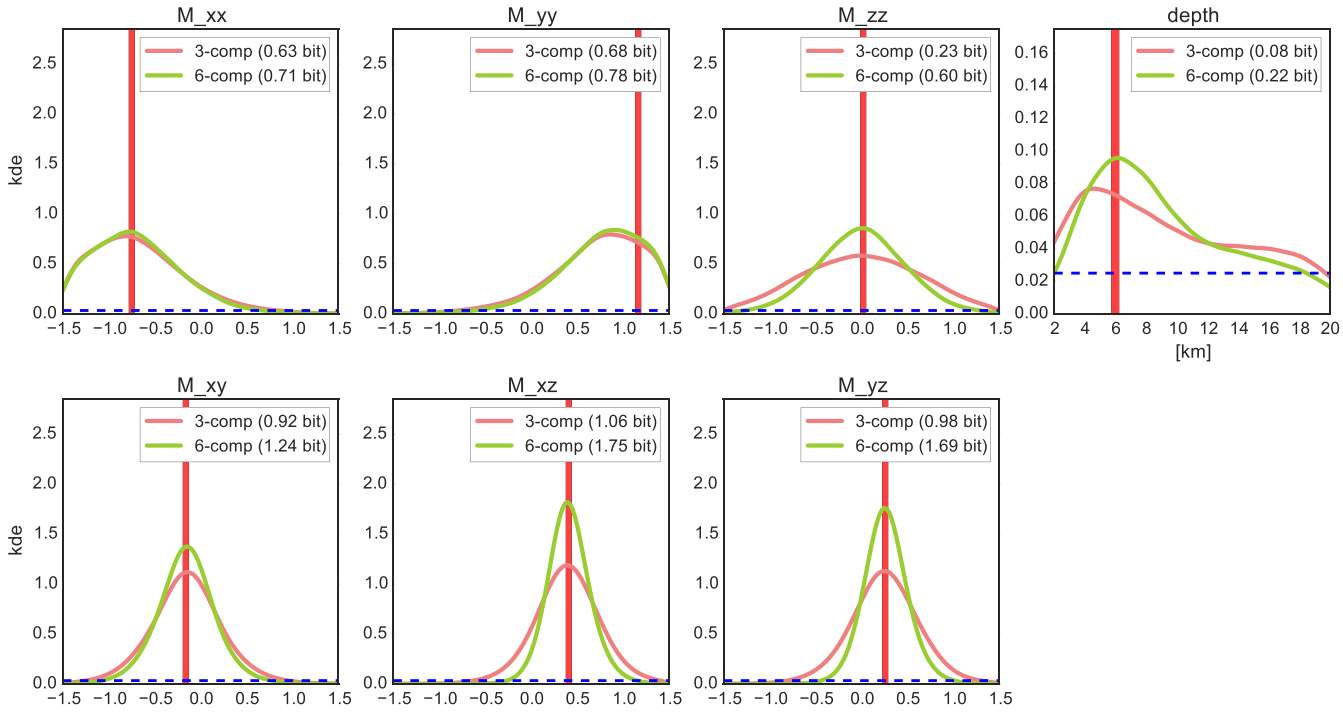

Figure 2. Inversion results for scenario I (theoretical stations). Each subplot belongs to one of the seven parameters inverted for and given on top of the subplot. Blue dashed line gives the *prior pdf*, while the orange and green lines give the *posterior pdf* for inversion of 48 3-C and 24 6-C stations, respectively. The pdf's are plotted as Gaussian kernel density estimates within the pre-defined range of values for the seven parameters. The red bar marks the true value of the target model.

providing a measure of how well a model **m** is fitting the data. Within the likelihood function the two types of data are weighted naturally by their noise level (compare eq. 5 in Bernauer *et al.* 2014). From the homogeneous *prior pdf* the *posterior pdf* is approximated by testing one million candidate models applying the Metropolis–Hastings algorithm. Roughly spoken, this algorithm can be described as random walk trough the model space. A candidate model is selected randomly from the parameter space (sampling the *prior pdf*), the forward problem is solved in the time domain according to eq. (2) and the waveforms are compared with the synthetic observations. Depending on the misfit value it is decided whether the random model is included in the solution ensemble. For further details on the algorithm, we refer to Metropolis & Ulam (1949), Metropolis *et al.* (1953) or to Hastings (1970).

To quantify the information content of the *posterior* relative to the *prior pdf,* we use Shannon's measure of information gain given as

$$I(\rho,\sigma) = \int \rho(x) \log\left[\frac{\rho(x)}{\sigma(x)}\right] dx. \qquad (4)$$

Due to the logarithm base 2 in eq. (4), the unit of the information gain is termed a *bit*. For further details on the method and Shannon's measure of information gain, we refer to the paper of Bernauer *et al.* (2014) and to Tarantola (2005).

4 EFFECTS OF INVERSION WITH AND WITHOUT CONSIDERATION OF ROTATIONAL GROUND MOTION DATA

In this section, we aim to recover the six components of the seismic moment tensor and the centroid depth of the synthetic earthquake described in Section 2 using the method described in Section 3. Further, we analyse the strike, dip, and rake angles as well as the percentages of DC, ISO, and CLVD components resulting from the decomposition of the obtained moment tensors.

We analysed two scenarios: In the first scenario, we studied the effects of inversion based on 48 conventional 3-C versus 24 novel 6-C theoretical stations. To generalize the results, we performed 1000 inversions based on random selection of stations out of a regular net (Fig. 1). In the second scenario, we compare the inversion results of theoretical data based on the real spatial distribution of stations of the INSN broad-band network of Iran.

At this point, we want to emphasize that the comparison of 3-C versus 6-C stations is based on the same number of seismograms within each scenario. Thus, we ensure that the results are not biased by the quantity of data used for inversion.

4.1 Scenario I: Inverting theoretical data of 48 3-C versus 24 6-C theoretical stations

In scenario I, we first inverted 3-C velocity seismograms at 48 theoretical stations evenly distributed around the location of the theoretical source (black dots and white-crossed dots in Fig. 1). The results are summarized in Fig. 2 where each subplot stands for one of the seven parameters inverted for and given on top of the subplots, namely the six components of the moment tensor and the centroid depth (epicentre is fixed). The *posterior pdf's* of the inversion based on 3-C stations are given as orange-coloured Gaussian kernel density estimations (*kde*) over the pre-defined range of parameter values. The information gains are given in the upper right corner of each subplot.

Except for the moment tensor components M_{xx} and M_{yy} the true values of the target model (indicated by red bars) could be resolved with well-defined peaks. For the component M_{xx}, the value of the target model is also resolved but with less defined peak. However, the standard deviations of the kernel density functions are relatively

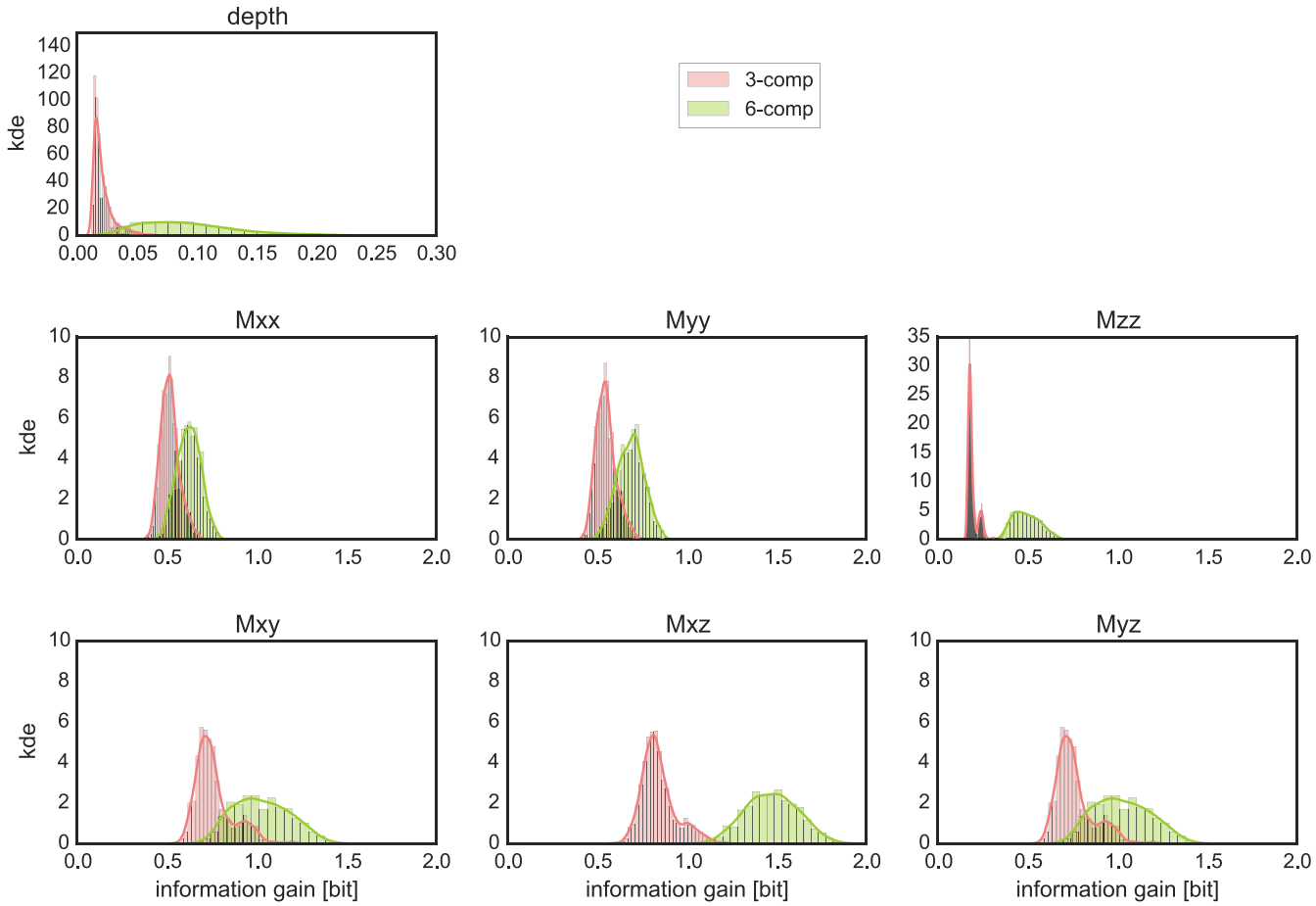

Figure 3. Gaussian kernel density estimations for the information gain corresponding to 1000 runs of scenario I. Coral and green distributions show the information gains from inverting 48 3-C and 24 6-C randomly chosen stations for the given parameters. The higher the information gain, the more the inversion benefits from using rotational motions. Same information gain means same inversion resolution using half the number of stations but the same amount of data.

large, especially for the component M_{zz} where the entire range of prior values lies within the distribution. The component M_{zz} also has a considerably lower information gain with 0.23 bit compared to 0.63–1.06 bit for the other components. For the centroid depth, the highest information gain is reached for a value of 4 km, which is too shallow compared to the true value. Also, the depth distribution is not purely Gaussian indicating a minor second peak at depth values of 16–18 km. With 0.08 bit the information gain is very low.

In Fig. 2, the green *kde*'s show the results of the inversion based on theoretical seismograms of 24 6-C stations. Compared to the inversion based on 3-C stations the overall information gain is now 53 per cent higher. Especially the components including spatial derivatives with depths benefit from the inversion of rotational ground motions. Component M_{zz} benefited by even 161 per cent ((0.60–0.23)/0.23 × 100 per cent). Also, the component M_{xy} benefited slightly with 35 per cent. Only the horizontal components M_{xx} and M_{yy} show almost no increase in resolution. Now, also the true value for the depth is better resolved. The minor peak at larger depth values is still visible but much more reduced. The determination of the centroid depth benefited by 175 per cent.

4.1.1 Generalization

Repeating the inversion procedure for 1000 randomly selected combinations of 48 3-C versus 24 6-C stations allows us to access the generality of our results. The random stations are selected out of a regular grid of theoretical station locations shown as grey dots in Fig. 1. The results of this random test are shown in Fig. 3. The orange and green colours again refer to the inversion of translational data only and translational plus rotational data, respectively. The Gaussian kernel density estimates are now plotted against the range of information gain. Therefore, a complete overlap of both *kde*'s can be interpreted as providing the same content of information/resolution. A shift of the curve to the right (to higher information gain) means a better resolution of the parameters inverted for. For all seven parameters the green *kde*'s, those from inverting translational and rotational ground motions together, distribute over a range of higher information gain values than the orange ones. Again, the components including spatial derivatives with depth benefit most while the components M_{xx} and M_{yy} show only a minor benefit. For the moment tensor component M_{xz} and M_{zz} both curves do not even show an overlap anymore. Thus, we could show that the promising results from one inversion shown in Fig. 2 can be generalized and are independent from the station distribution. However, the very wide distribution over the information gain for depth based on six-component data indicates that this is still a sensitive parameter to be inverted for.

4.1.2 Decomposition

For many applications the source angles strike, dip, and rake (describing the tectonic mechanism of the source) are much more

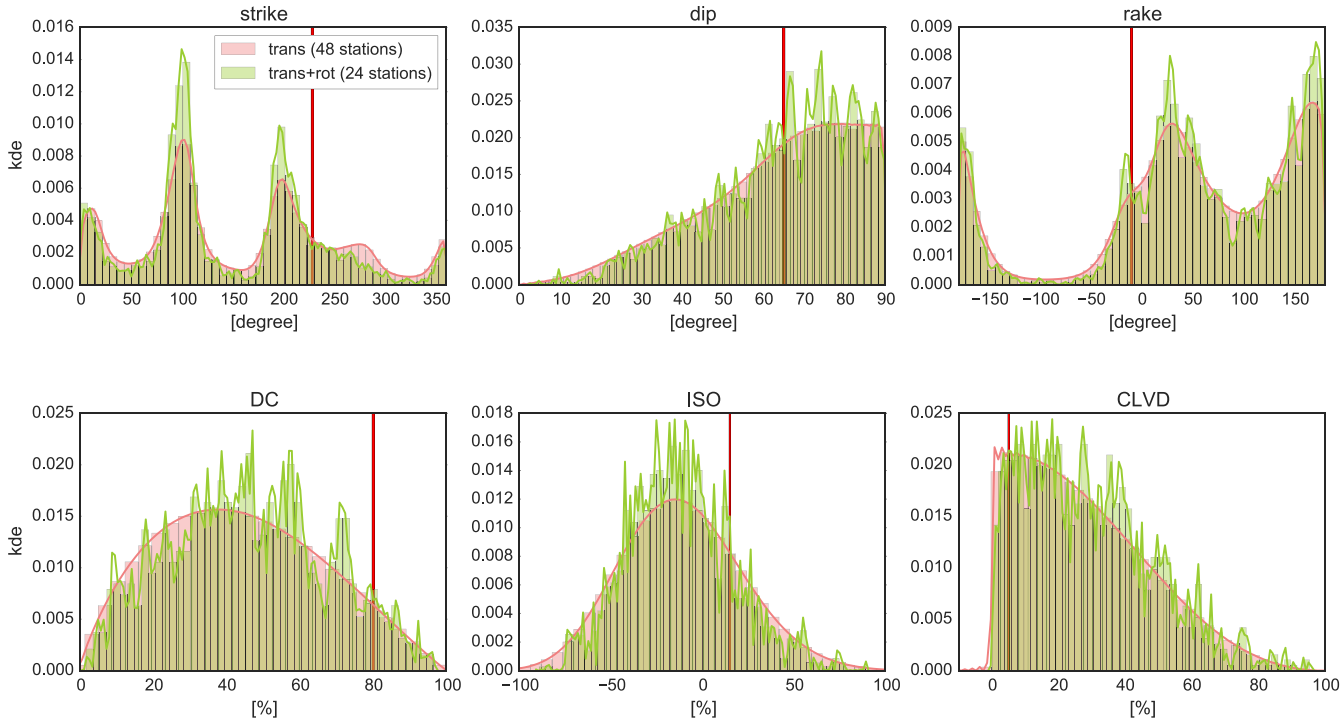

Figure 4. Gaussian kernel density estimations for fault angles and source contribution percentages of decomposed moment tensors corresponding to 1000 runs of scenario I. The red, vertical bar shows the true value of the target source.

important than the moment tensor itself. Also, the percentage of the DC, ISO, and CLVD parts of the moment tensor are used to, for example, discriminate tectonic events from others or analyse magma flow in volcanic regions. Therefore, we decompose each of the resulting moment tensors from the generalized 1000 inversions (i.e. 1e9 moment tensors). For the decomposition, we applied the method of Jost & Herrmann (1989) to derive the ISO and deviatoric part of the moment tensor. The deviatoric part is further decomposed into a DC and a CLVD part. Thus, we obtain new distributions for the six derived parameters (ISO, DC, CLVD, strike, dip and rake), containing 1e9 values each, for which we show the *kde*'s in Fig. 4. The colour-coding is the same as in Figs 2 and 3. The values of the target model are marked with red bars. The subplots for the strike, dip, and rake angles show the values for both nodal planes. Therefore, they contain twice as much values as the subplots for the DC, ISO and CLVD percentages.

The first eye-catching feature is the strong scatter within the entire parameter ranges for all six parameters. We will further discuss this later in the text. Secondly, the results from the six-component data are less smooth than the one from the three-component data. Although the overall distribution for, for example, the DC percentages are roughly the same for both, the results from the six-component data show a stronger scatter with sub-peaks at higher DC values than the results from the three-component data. The same effect is also visible for ISO percentages and the dip and rake angles with sub-peaks at the values of the target model (compare Table 1).

The subplot for the strike angle shows two very distinct peaks, one at about 190° and one at about 100°. These are the angles for the source and auxiliary plane, respectively, and therefore refer to the same mechanism. Compared to the true model, the favoured mechanism from inversion ($\phi = 190°$, $\delta = 75°$, $\lambda = -10°$) is rotated by less than 40° from an NE–SW to an NNE–SSW oriented fault plane and has a steeper dip but generally remains a strike-slip. Altogether, we can say that the chances to derive the real mechanism and source type are much higher from combining translational and rotational ground motion than inverting translational data alone.

4.2 Scenario II: Inverting theoretical data of 20 3-C versus 10 6-C real Iranian broadband stations

To make the study more realistic, in scenario II, we based our theoretical inversion on the real station distribution of the INSN network of Iran (red triangles in Fig. 1). In total, there are 20 station locations available. Therefore, we compared the results of inversion based on purely translational ground motion of all available stations versus inversion based on 10 assumed 6-C stations out of these 20 stations. These 10 stations have been chosen randomly again. The result of this comparison is shown in Fig. 5.

In general, the very good results based on the theoretical station distribution of scenario I are confirmed. The information gain for all six moment tensor components more than doubled. Again, especially the moment tensor components including spatial derivatives with depth benefit most from including rotational ground motions. The increase of the overall information gain is now even 136 per cent.

The benefit of including rotational ground motion for determining the centroid depth this time is 50 per cent. Inverting only translational ground motions of all 20 stations resulted in a wrong depth of 18 km with a second minor peak at 4 km. Inverting both, translational and rotational ground motions, still result in two possible centroid depths. However, the major peak is now at about 5 km and thus much closer to the true value of 6 km. Compared to the inversion of ground motions from the theoretical station distribution in scenario I, the resolution of depth determination is worse for both inversions. We suspect this effect to be an effect of station distribution, probably caused by the large azimuthal gap to the north due to the South Caspian Basin.

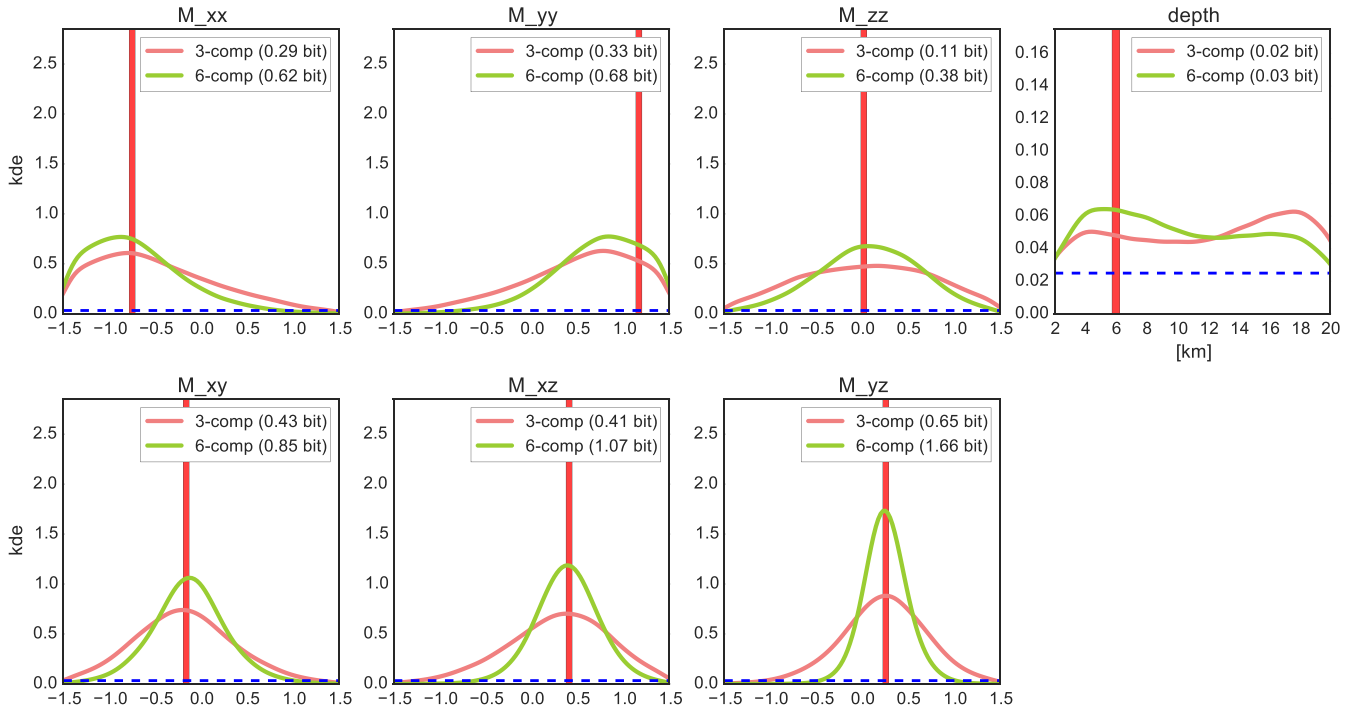

Figure 5. Inversion results for scenario II (real station distribution). Each subplot belong to one of the seven parameters inverted for and given on top of the subplot. Blue dashed line gives the *prior pdf*, while the orange and green lines give the *posterior pdf* for inversion of 20 3-C and 10 6-C stations, respectively. The pdf's are plotted as Gaussian kernel densities within the pre-defined range of values for the seven parameters. The red bar marks the true value of the target model.

5 DISCUSSION

In this theoretical study, we purposely selected one of the most difficult source cases to invert for: a shallow strike-slip event (depth $\ll$ wavelength) of medium-sized magnitude ($M_w = 4.0$) in a regional distance range (about 200 to 1000 km). We tested whether and how much the inversion for seismic point sources can benefit from the availability of rotational ground motion data.

5.1 Resolvability of moment tensor

It is very well known that the moment tensor components M_{xz} and M_{yz} are usually poorly resolved from the inversion of translational ground motion data in the regional distance range (Bukchin 2006; Bukchin *et al.* 2010). The reason lies in the equation for the radiation pattern of the surface waves which are usually used in this distance range. Both, Love and Rayleigh wave radiation patterns, contain terms including spatial derivatives of the eigenfunctions with respect to depth with coefficients M_{xz} and M_{yz}. For very shallow sources (depth $\ll$ wavelength) these terms tend to zero because they vanish at the free surface due to their proportionality to a shear traction on a horizontal plane. However, depending on the conditions of the study region also other moment tensor components can show considerable instabilities.

Rotational ground motions are linear combinations of the space derivatives of the translational ground motions (see eq. 1). At the Earth's surface the horizontal components correspond to tilt. Tilt contains information on the seismic wavefield at depth (the velocity gradient with depth) which is not available from translational ground motion. Thus, rotational motion provides an additional constraint, especially useful for determining the off-diagonal moment tensor components and the centroid depth of the source. Also, the immensely increased resolution for the component M_{zz} is understandable intuitively. It is connected to the vertical strike-slip mechanism of the target event which theoretically does not contain vertical displacement in the translational data. However, in the rotational data this component stands for rotation around the vertical axis which indeed theoretically should show large amplitudes for a vertical strike-slip.

In Fig. 6, we exemplary show the waveform fit of synthetic data with forward calculated waveforms from resulting moment tensors of scenario II in the range of the lowest misfit plus 10 per cent for the station ASAO (WSW of the source). These are about 7430 waveforms with a generally very good fit to the data. Because the phases are already in good agreement, the figure suggests that the benefits due to incorporating rotational ground motion mainly come from their amplitudes.

5.2 Resolvability of derived parameters

To derive the different source type percentages and the source angles the moment tensor needs to be decomposed. There are several ways to do so and for an overview we refer to Jost & Herrmann (1989). For seismotectonic, volcanic and geothermal studies, usually the decomposition into DC (tectonic part), ISO (volumetric changes) and CLVD is used. The first step in the process of decomposition is to determine the ISO part of the moment tensor which is defined as 1/3 of the trace (sum of eigenvalues) of the matrix. That means only the diagonal elements of the moment tensor are influenced by this step. The further decomposition is then based on the deviatoric moment tensor defined as full moment tensor minus ISO part. Therefore, the entire decomposition depends on the reliable estimation of the ISO part. As shown in Figs 2 and 5, two of the three diagonal elements (M_{xx} and M_{yy}) show deficiencies in their resolution. For M_{yy} the peak of the *posterior pdf* does not even match the value of the

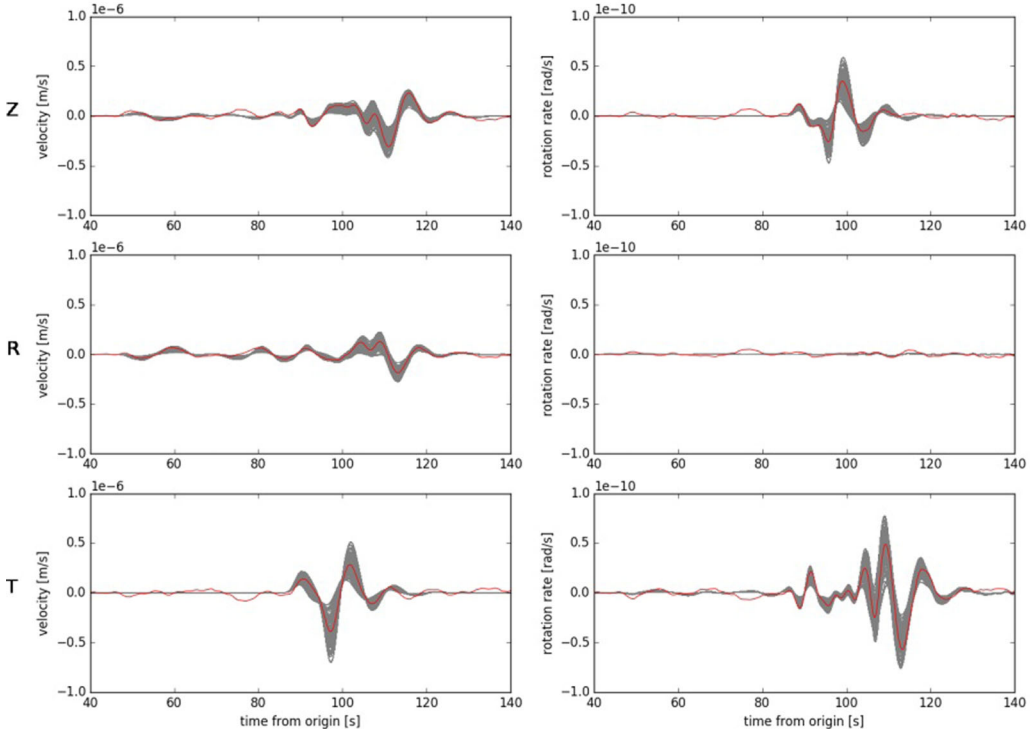

Figure 6. Waveform comparison of the synthetic data perturbed with Gaussian noise (red) and waveforms of resulting moment tensors (grey) within a range of 10 per cent from the lowest misfit (∼7430 waveforms) from inversion of scenario II. Left and right sides show three components of translation and rotation for station ASAO (WSW of the source), respectively.

target model. These discrepancies explain the difference between the target value and the peaks of the distributions for the ISO part in Fig 4. Based on the improper determination of the ISO part, the further decomposition must be flawed.

An additional explanation for the deficient decomposition comes from the Bayesian approach itself. The inversion for the parameters of a point source is a complex task (multiparameter problem) which is further hampered by the quality of the available data (noise, source depth, station geometry, etc.). The risk to get a wrong solution from a deterministic inversion is high. This risk is evaded by applying the Bayesian inversion. However, the disadvantage is that we cannot provide an distinct solution anymore but obtain a family of solutions (*posterior pdf's*). Such a family of solutions hampers the further processing of the results, in this case the determination of source angles and mechanism percentages. A large variance in these parameters is due to a low resolution of single inversion parameters (low information gain, flat curve for the *posterior pdf*). This effect seems to apply here.

By including the rotational data into the inversion we are able to improve the resolution of the single inversion parameters significantly (i.e. moment tensor components and centroid depth). However, due to the complexity of the problem their resolution seems to be still insufficient for decomposition and strongly dependent on the geometry of the stations around the source. A pre-selection or sorting of moment tensors, for example, according the lowest misfit, before the decomposition may solve this difficulty but includes a high risk to introduce biases if not done carefully.

5.3 Resolvability of centroid depth

Inversion for moment tensors is very sensitive for centroid depth and a false assumption of depth can lead to a completely wrong mechanism (Šílený *et al.* 1992). Typically, the centroid depth is determined by performing the inversion assuming different depths sampling an appropriate depth range. The depth with the lowest inversion residual is then assumed to be the centroid depth. However, this procedure not always provides a clear and unambiguous result. Even for a quite optimal distribution of stations as in scenario I, the depth is determined wrongly with an obscure peak for the *kde* from inverting translational data alone (Fig. 2).

It is very intuitive that the information on the vertical displacement gradient within the rotational ground motion data improves the resolution of the depth drastically. However, from the results of scenario II (Fig. 5), it seems that another factor is more important for the resolution of centroid depth than the kind of data. Here, both inversions, with and without rotational ground motion, show deficiencies. For the inversion of translational data alone it is even wrong by 14 km. We assume that this may be an effect of the station distribution around the source with respect to geometry, azimuth, and distance. Due to the SCB alone there is an azimuthal gap of 91° to the north of the source. Then, at the western side of the source there are almost twice as much stations located as on the eastern side.

Interestingly, the ambiguity in depth with one possible solution in very shallow depth ($h \leq 6$ km) and another one at the lower end of the seismogenic zone of Iran ($h > 17$ km) is also visible in the real world. Moment tensor studies in the Alborz mountains and in the NW part of Iran have shown exactly the same effect (Donner *et al.* 2013, 2015).

The results of the generalization of scenario I (Fig. 3) give additional indications for the station distribution being the discriminating factor. The red *kde* for the inversion of translational data shows a very narrow and distinct peak at quite low values for information gain. We can assign this effect to the not very high resolvability

of centroid depth by the data. In contrast, the *kde* for the inversion of both ground motion data shows a very flat distribution over a wide range of values for the information gain. Neither the number of data nor the parameters of the inversion within the 1000 performances underlying this *kde* changed. The only parameter changing is the (randomly selected) spatial distribution of the used stations. Nevertheless, to fully understand the effect of station distribution it needs further tests which is not the purpose of this study. For this study we aimed to show the remarkable benefits for the resolution of the moment tensor when inverting translational ground motion data together with rotational ones.

6 CONCLUSIONS

In this study we assessed the advances of inversion for seismic moment tensors from six-component waveforms (translational and rotational ground motions) compared to the conventional inversion of three-component translational ground motions only. The study is based on a series of Bayesian inversions for different sets of theoretical and real station distributions in Iran. We could show that the inclusion of rotational ground motion data significantly increase the resolution of the inversion parameters, that is, the six components of the full moment tensor and the centroid depth. Especially, the components including spatial derivatives with depth and the centroid depth have the highest potential to benefit from rotational ground motions. Their information gain increased by more than 100 per cent. We assume the horizontal components of the rotation vector to be responsible for this increase in information. They include information on the vertical displacement velocity gradient which is not available from translational ground motion data.

ACKNOWLEDGEMENTS

Large parts of this study have been done using ObsPy (ObsPy 0.10.1 2015; Beyreuther *et al.* 2010; Megies *et al.* 2011; Krischer *et al.* 2015) and we are very thankful to the developers. The research presented in this paper was funded by the European Research Council (Project: ROMY). The numerical computations were performed on the National Supercomputer SuperMUC maintained by the Leibniz-Rechenzentrum (Project: h019z). We also thank Ivan Lokmer and a second reviewer for their valuable comments which helped to improve this manuscript.

REFERENCES

Aki, K. & Richards, P.G., 2002. *Quantitative Seismology,* 2nd edn, University Science Book.

Bean, C., Lokmer, I. & O'Brien, G., 2008. Inversion of near-surface volcanic structure on long-period seismic signals and on moment tensor inversion: simulated examples from Mount Etna, *J. geophys. Res.,* **113,** B08308, doi:10.1029/2007JB005468.

Berberian, M., 2014. *Earthquakes and Co-seismic Surface Faulting on the Iranian Plateau,* Elsevier.

Bernauer, F., Wassermann, J. & Igel, H., 2012. Rotational sensors—a comparison of different sensor types, *J. Seismol.,* **16,** 595–602.

Bernauer, M., Fichtner, A. & Igel, H., 2014. Reducing nonuniqueness in finite source inversion using rotational ground motions, *J. geophys. Res.,* **119,** 4860–4875.

Beyreuther, M., Barsch, R., Krischer, L., Megies, T., Behr, Y. & Wassermann, J., 2010. ObsPy: a python toolbox for seismology, *Seismol. Res. Lett.,* **81,** 530–533.

Bukchin, B., 2006. Specific features of surface wave radiation by shallow sources, *Phys. Solid Earth,* **42,** 712–717.

Bukchin, B., Clévédé, E. & Mostinskiy, A., 2010. Uncertainty of moment tensor determination from surface wave analysis for shallow earthquakes, *J. Seismol.,* **14,** 601–614.

Donner, S., Rößler, D., Krüger, F., Ghods, A. & Strecker, M.R., 2013. Segmented seismicity of the Mw 6.2 Baladeh earthquake sequence (Alborz mountains, Iran) revealed from regional moment tensors, *J. Seismol.,* **17,** 925–959.

Donner, S., Krüger, F., Rößler, D. & Ghods, A., 2014. Combined inversion of broad-band and short-period waveform data for regional moment tensors: a case study in the Alborz mountains, Iran, *Bull. seism. Soc. Am.,* **104,** 1358–1373.

Donner, S., Krüger, F., Rößler, D. & Ghods, A., 2015. The Ahar-Varzeghan earthquake doublet (M_w 6.4 and 6.2) of 11 August 2012: regional seismic moment tensors and a seismotectonic interpretation, *Bull. seism. Soc. Am.,* **105,** 791–807.

Dufumier, H. & Cara, M., 1995. On the limits of linear moment tensor inversion of surface wave spectra, *Pure appl. Geophys.,* **145,** 235–257.

Fichtner, A., Kennett, B.L.N., Igel, H. & Bunge, H.-P., 2009. Spectral-element simulation and inversion of seismic waves in a spherical section of the Earth, *J. Numer. Anal. Ind. Appl. Math.,* **4,** 11–22.

Hastings, W.K., 1970. Monte Carlo sampling methods using Markov chains and their applications, *Biometrika,* **57,** 97–109.

Jost, M.L. & Herrmann, R.B., 1989. A student's guide to and review of moment tensors, *Seismol. Res. Lett.,* **60,** 37–57.

Krischer, L., Megies, T., Barsch, R., Beyreuther, M., Lecocq, T., Caudron, C. & Wassermann, J., 2015. ObsPy: a bridge for seismology into the scientific Python ecosystem, *Comput. Sci. Discovery,* **8,** 014003, doi:10.1088/1749-4699/8/1/014003.

Maps of the World, 2013. Political map of Iran. Available at: http://www.mapsofworld.com/iran/iran-political-map.html, last accessed 11 November 2015.

Megies, T., Beyreuther, M., Barsch, R., Krischer, L. & Wassermann, J., 2011. ObsPy - What can it do for data centers and observatories, *Ann. Geophys.,* **54,** 47–58.

Metropolis, N. & Ulam, S., 1949. The Monte Carlo method, *J. Am. Stat. Assoc.,* **44,** 335–341.

Metropolis, N., Rosenbluth, M.N., Teller, A.H. & Teller, E., 1953. Equation of state calculations by fast computing machines, *J. Chem. Phys.,* **21,** 1087–1092.

ObsPy Development Team, 2015. ObsPy 0.10.1, doi:10.5281/zenodo.16248.

Pasyanos, M.E., Matzel, E.M., Walter, W.R. & Rodgers, A.J., 2009a. Broad-band Lg attenuation modelling in the Middle East, *Geophys. J. Int.,* **177,** 1166–1176.

Pasyanos, M.E., Walter, W.R. & Matzel, E.M., 2009b. A simultaneous multiphase approach to determine *P*-wave and *S*-wave attenuation of the crust and upper mantle, *Bull. seism. Soc. Am.,* **99,** 3314–3325.

Schreiber, K.U., Velikoseltsev, A., Carr, A.J. & Franco-Anaya, R., 2009. The application of fiber optic gyroscopes for the measurement of rotations in structural engineering, *Bull. seism. Soc. Am.,* **99,** 1207–1214.

Šílený, J., Panza, G.F. & Campus, P., 1992. Waveform inversion for point source moment tensor retrieval with variable hypocentral depth and structural model, *Geophys. J. Int.,* **109,** 259–274.

Statistical Centre of Iran, Office of the Head Public Relations and Internal Cooperation 2012. Selected findings of national population and housing census 2011. Available at: www.amar.org.ir/Default.aspx?tabid=500, last accessed 11 November 2015.

Tarantola, A., 2005. *Inverse Problem Theory and Methods for Model Parameter Estimation,* 2nd edn, SIAM.

Zamani, A. & Agh-Atabai, M., 2009. Temporal characteristics of seismicity in the Alborz and Zagros regions of Iran using a multifractal approach, *J. Geodyn.,* **47,** 271–279.